Hue University Journal of Science: Natural Science; ISSN 1859-1388

Vol. 126, No. 1C, 2017, P. 29-36; DOI: 10.26459/hueuni-jns.v126i1C.4216

ULTRASOUND-ASSISTED SYNTHESIS OF MAGNETITE NANOPARTICLES BY CO-PRECIPITATION METHOD

Thanh Q. Bui*, Suong N. C. Ton

HU – University of Sciences, 77 Nguyen Hue St., Hue, Vietnam

Abstract: The conventional co-precipitation method of the synthesis of magnetite (Fe_3O_4) nanoparticles has been procedurally and ultrasonically altered. The effects of NH_3 solution adding paths to the precursor solution, and ultrasonic assistance were indicated and demonstrated through specific experiments. Suggested explanations for observed phenomena were provided. Characteristic information has proved the enhanced performance of the alternative procedure. The magnetite nanoparticles possess a uniform nano-crystallised spherical morphology, narrow small-sized distribution (10 nm), high magnetisation (57.7 emu·g^{-1}), and negligibly low coercivity (5 Oe).

Keywords: Fe_3O_4, co-precipitation method, magnetite nanoparticles, ultrasonic, superparamagnetism

1 Introduction

Nano-sized materials have been of scientific and technological interest because of their unique properties, i.e., very large surface area and high characteristic reactivity, that differ from their corresponding bulk states. Magnetic nanoparticles, especially magnetite (Fe_3O_4), possess numerous potential applications in magnetic recording technology, pigments, catalysis, photocatalysis, medical uses, and environmental processes [15] due to their good biocompatibility, strong superparamagnetic property, low toxicity, and easy preparation [4]. In biomedical applications, the magnetite nanoparticles have been applied in various fields, such as targeted drug delivery, hyperthermal treatment, cell separation, magnetic resonance imaging, immunoassay, and separation of biomedical products [5, 13]. Most of the mentioned biochemical applications require magnetite nanoparticles with chemical stability, biocompatibility, biologically coherent size, and firm superparamagnetic property [20]. Therefore, besides small sizes for better mobility and fluidity in the bio-medium, synthesized magnetite nanoparticles also need to perform paramagnetic property for magnetic-targeted transmission and superparamagnetism for magneto-thermal transformation purposes [2, 7].

Magnetite, well-known as the strongest magnetic mineral in nature, has attracted diverse research works and applications [6, 18]. Hence, many preparation methods of magnetite nanoparticles have been developed and published in varied research papers, such as co-precipitation, hydrothermal synthesis, solvothermal synthesis, sonochemical synthesis, and micro-emulsion. Co-precipitation is the simplest and most efficient synthesis route to obtain the magnetic particles, based on the following reaction: $Fe^{2+} + 2Fe^{3+} + 8OH^- \rightarrow Fe_3O_4 + 4H_2O$ [9]. In co-precipitation, a

** Corresponding: thanh.qt.bui@husc.edu.vn*

Submitted: 26-4-2017; Revised: 14-9-2017; Accepted: 28-9-2017

stoichiometric mixture of ferrous and ferric precursors in an aqueous medium is used as an iron source that yields the superparamagnetic nanoparticles after introducing an alkaline solution into the mixture. However, the size distribution of as-prepared nanoparticles by co-precipitation is relatively broad due to the presence of both nucleation and particle growth throughout the synthesis process [5].

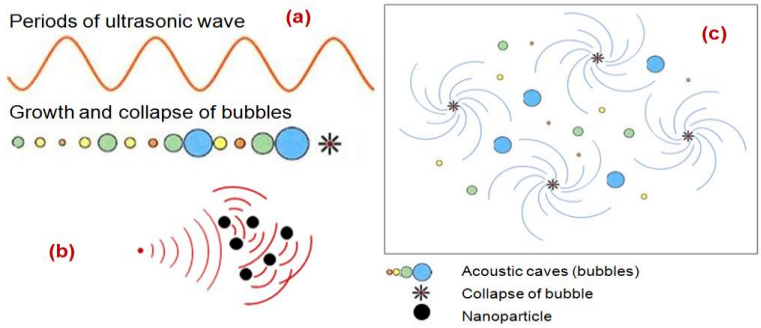

Fig. 1. Illustrations of ultrasonic properties in liquid medium: (a) Formation and collapse of acoustic cavitation (bubbles) along with periods of ultrasonic wave, (b) Mechanical micro-interaction properties on suspended particles, and (c) Vigorously circulatory micro-streams

The sonochemical technique arises from acoustic cavitation phenomena, formation, growth, and collapse of bubbles in the liquid medium (Fig. 1a). The extremely high temperature (~ 5000 K), pressure (~ 20 MPa), and very high heating/cooling rates (~ 10^{10} $K \cdot s^{-1}$), coming from the collapse of the bubbles, create a unique reacting condition of thermal and pressured dispersion [1]. Besides, the oscillating bubbles in the ultrasonic field produce vigorous circulatory motions in their surrounding fluid, called micro-streams (Fig 1c), which occur continuously and entirely in the medium, creating uniform concentrations of the reactants [11]. Also, by exhibiting mechanical micro-interaction properties, ultrasound could impinge on a suspended object [19], functioning as a surface protection solution at the micron-scale or even nano-scale (Fig. 1b). Therefore, ultrasound has considerably high potentials for small-sized research generally, and nanomaterials specifically.

In this study, co-precipitation-based experiments in the synthesis of magnetite nanoparticles have been procedurally processed to mainly demonstrate the formation of an ultrasonic environment and its influence inside the reacting medium through explaining characteristic results. Besides, the introduction of a basic solution into the ferrous precursor has also been examined.

2 Experiments

2.1 Chemicals and reacting conditions

Ferrous chloride tetrahydrate ($FeCl_2.4H_2O$), ferric chloride hexahydrate ($FeCl_3.6H_2O$), hydrochloric acid (HCl, 37 %), and ammonia solution (NH_3, 28 %) were of analytical grade and purchased from Xilong Chemical Co., Ltd. All chemicals were used without further purification. In all experiments, reactant solutions were deoxygenated by nitrogen bubbling for 30 minutes before use. Ultrasonic condition (Cole-Parmer-8892, USA) was performed at 42 KHz, 100 W.

2.2 Preparation of Fe_3O_4 nanoparticle samples

Fe_3O_4 nanoparticles were synthesized using a coprecipitation-based method following 3 procedures, and the samples were notated with M-01, M-02, and M-03. In a typical synthesis procedure, 1.5 mmol $FeCl_2.4H_2O$ and 3.0 mmol $FeCl_3.6H_2O$ were dissolved in 50 mL deoxygenated distilled water. 10 mL ammonia was differently added to the iron precursor solutions at 40 °C, bubbling with N_2 under mechanical stirring and ultrasonic radiation. The reacting conditions were kept further 30 minutes for crystallising and aging. Table 1 briefs the synthesis procedures of M-01, M-02, and M-03 experiments, respectively.

Table 1. Briefs of experimental differences of M-01, M-02, and M-03

Sample	Ammonia introduction	Assistance solution
M-01	Droplet	Mechanical stir
M-02	Pouring	Mechanical stir
M-03	Pouring	Ultrasonic radiation

The black Fe_3O_4 precipitates were isolated from the solutions using magnetic decantation and washed with deoxygenated distilled water several times, then dried in an oven at 70 °C.

2.3 Characterisation

The crystal phase of products was characterised using X-ray diffraction (XRD, D8-Advance-Bruker, Germany equipped with Cu Kα radiation, λ = 1.5406 Å), and the mean crystalline size of nanoparticles was calculated using Scherrer's equation based on XRD data [12, 14]. The morphology of the synthesized products was observed with transmission electron microscopy (TEM, JEOL-1010, Japan). The magnetic properties were investigated through collected magnetisation-hysteresis (M-H) curves using vibrating sample magnetometer equipment (VSM, PPMS-6000, USA) at room temperature. The elemental analysis was carried out using energy dispersive X-ray spectroscopy (EDX, JEOL-6490-JED-200, Japan).

3 Results and discussion

XRD patterns are used to demonstrate the crystal structure of the samples (Fig. 2). The diffraction angles are consistent with those from the standard XRD pattern of magnetite (Fe_3O_4, JCPDS card No. 00-001-1111) with no extra peaks observed. Five clear characteristic peaks at 30.5 ° (200), 35.9 ° (311), 43.5 ° (400), 57.3 ° (511), and 63.1 ° (440), and the distance of the lattices calculated and referenced indicate that all samples possess the inverse cubic spinel structure of magnetite with over 99 % of similarities with the standard pattern (Table 2). The average grain size of magnetite nanoparticles for M-01, M-02, and M-03 samples, calculated from Scherrer's equation with full-width at half-maximum values obtained from the strongest peak (311), is 26.5 nm, 7.6 nm, and 7.7 nm, respectively. In addition, the XRD patterns of M-02 and M-03 samples have low intensity and broad reflections, and this indicates the decrease of the grain size of the nanoparticles, leading to X-rays being more strongly and widely diffused than the one observed from M-01 sample [16].

Table 2. Lattice distance of M-01, M-02, and M-03 samples and magnetite standard (Fe_3O_4, JCPDS card No. 00-001-1111)

hkl	M-01		M-02		M-03		Magnetite standard
	d (Å)	Similarity (%)	*d* (Å)	Similarity (%)	*d* (Å)	Similarity (%)	*d* (Å)
200	2.954	99.56	2.958	99.70	-	-	2.967
311	2.519	99.49	2.524	99.68	2.521	99.57	2.532
400	2.089	99.52	2.089	99.52	2.096	99.86	2.099
511	1.610	99.69	1.611	99.75	-	-	1.615
440	1.476	99.80	1.477	99.85	1.478	99.93	1.479

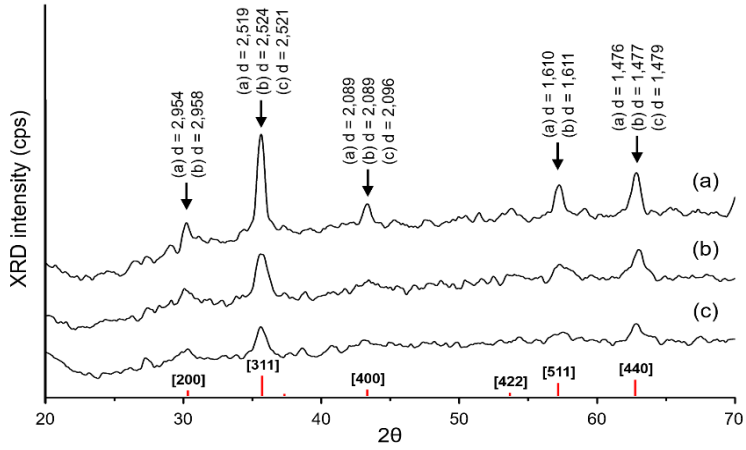

Fig. 2. XRD patterns and lattice distances of (a) M-01, (b) M-02, and (c) M-03

TEM images reveal the morphology and size distribution of as-prepared nanoparticles (Fig. 3). An unidentified morphology with a wide range of size distribution, from tens to hundreds nanometres, appears on the M-01 sample (Fig. 3a, 3b). Meanwhile, samples M-02 (Fig. 3c, 3d) and M-03 (Fig. 3e, 3f) have even spherical nanoparticles with an average diameter of around 10 nm in the form of aggregates. The larger particle size compared with that calculated from XRD data could be explained by the inhomogeneous strain and crystal lattice imperfections on the surface of the nanoparticles [21]. Besides, in aqueous suspensions, a combination of Lifschitz-van-der-Waals and magnetic forces would result in magnetite nanoparticles that tend to aggregate into considerably large nanoparticle clusters (> 1 μm) [17] instead of discretely single-domain individual nanoparticles.

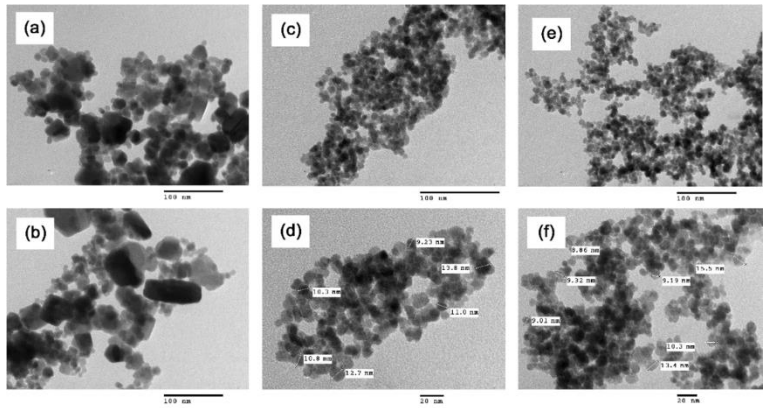

Fig. 3. TEM images of (a-b) M-01, (c-d) M-02, and (e-f) M-03

The heterogeneous morphology of the M-01 sample might be due to the simultaneous crystalline nucleation and crystalline growth throughout the synthesis process [10]. These two processes take place when ammonia was slowly added to the precursor solution. This leads to the formation and growth of multi-magnetic-moment crystalline magnetite particles (Fig. 4a). In contrast, pouring ammonia rapidly into the reactant solution makes the medium state to reach the solubility threshold and pass over the growth process [10], leading to an entire mass nucleation [10] with small mono-sized distributed nanoparticles as seen in the M-02 and M-03 samples. However, the synthesised nanoparticles without a proper surface protection would crystallise onto the surface of already-formed particles and form multi-magnetic moments in a crystalline domain. This, in turn, decreases the response of the nanoparticles to the alternative external magnetic field applied to study the superparamagnetic property [8]. Unfortunately, the crystalline aggregation is not recognisable by TEM and XRD analyses.

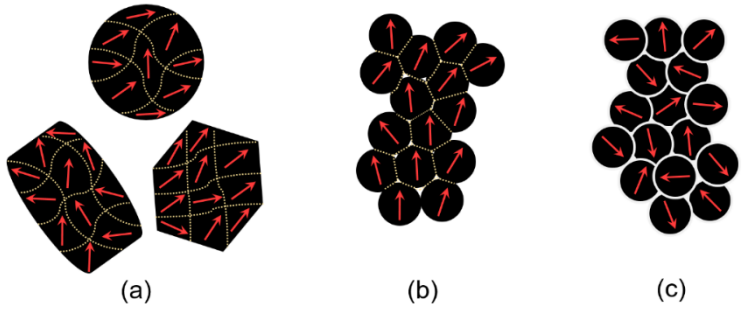

Fig. 4. Illustrations of (a) Multi-magnetic-moment crystalline magnetite particles, (b) Magnetite micro-scale clusters containing crystalline domains with multi-magnetic moments inside, and (c) Single-crystalline magnetite domains with single-magnetic moments

Fig. 5 shows the room-temperature M-H curves of as-prepared magnetite nanoparticles, measured by cycling the external magnetic field between -12000 Oe and 12000 Oe. All the samples exhibit soft magnetic characteristics with high saturated mass magnetisation (Ms) values of 72.5 emu·g^{-1} for M-01, 67.7 emu·g^{-1} for M-02, and 57.7 emu·g^{-1} for M-03. Meanwhile, the coercivity is

considerably different with 75 Oe, 25 Oe, and 5 Oe for M-01, M-02, and M-03 samples, respectively. The relatively high coercivity value of the M-01 sample is inferred from the over-threshold particle size for superparamagnetism, (~ 25 nm) of magnetite materials [3]. A negligible coercivity value (weakest magnetic resistance) of the M-03 sample could be due to the fact that the as-prepared small and discrete magnetite nanoparticles contain single-crystalline domains with single-magnetic moments, and they are freely affected by an external magnetic field and instantaneously respond to the magnetic alternatives (Fig. 4c). This indicates that this sample retains its superparamagnetic property after the synthesis was completed. The medium magnetic resistance of the M-02 sample suggests the occurrences of crystalline aggregates that cause the formation of larger magnetite micro-scale clusters containing crystalline domains with multi-magnetic moments; these moments might resist each other from responding properly to the applied magnetic field (Fig. 4b).

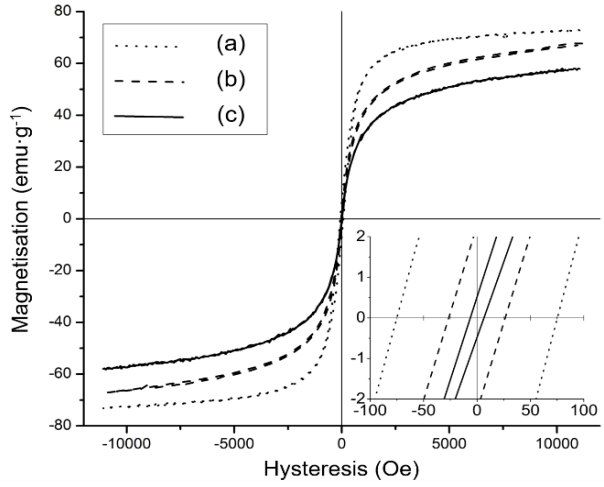

Fig. 5. Room-temperature M-H curves of (a) M-01, (b) M-02, and (c) M-03

Unique micro-effects of ultrasonic waves could be utilised to explain the observed difference of the magnetic properties between samples M-02 and M-03. The waves create a uniform condition of the thermal and pressured dispersion throughout the reacting medium. They also serve as a diffusion technique and a surface protection. Firstly, the micro-stream appearing in the micro-scale, which comes from the collapse of the acoustic bubbles in the liquid medium, can form a microscopically homogeneous state throughout the bulk solution. This would lead to a small and uniform-sized distribution of the synthesized magnetite nanoparticles. In addition, by virtue of mechanical nature, the wave radiation would physically interact right with the surface of newly co-precipitated nanoparticles, preventing inter-surface crystallisation. The interaction could be considered as a mechanical surface protection, keeping the nanoparticles suspended apart in the reaction medium. As a result, the products appear as discrete magnetite nanoparticles containing only one magnetic moment in one crystalline domain.

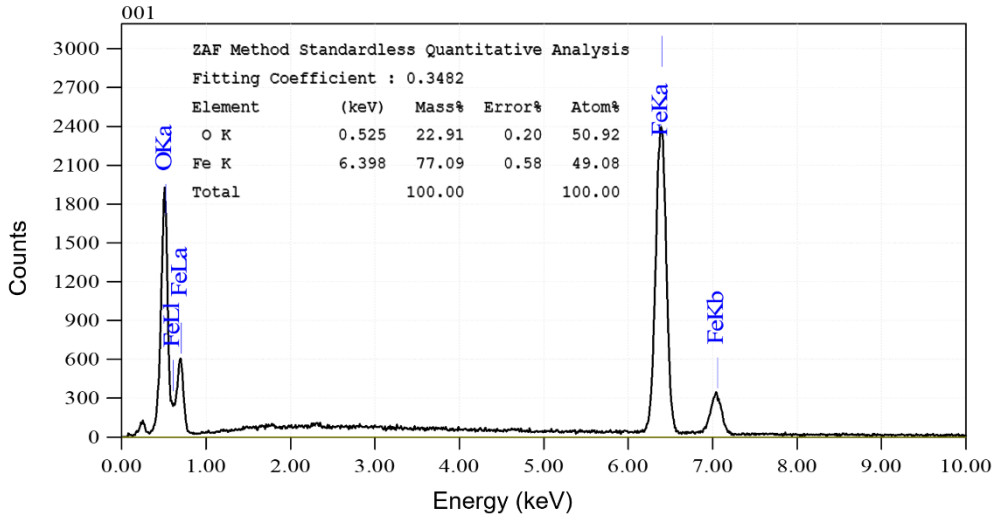

Fig. 6. EDX spectrum and elemental analysis of M-03

The EDX spectrum of M-03 sample (Fig. 6) shows only characteristic peaks of Fe and O, indicating that iron oxide was successfully synthesised. The material contains only Fe (77.09 %) and O (22.91 %).

4 Conclusion

The utilisation of ultrasonic micro-effects as a diffusion technique and a surface protection can enhance the conventional co-precipitation method in the synthesis of magnetite nanoparticles. The as-prepared magnetite product is uniform nano-crystallised spherical particles with a narrow small-sized distribution. The material is single-magnetic-moment nanoparticles with small coercivity and instantaneously responds to the external magnetic changes. The method could be an alternative for the small-sized material synthesis.

References

1. Dang F., Enomoto N., Hojo J., Enpuku K. (2010), Sonochemical coating of magnetite nanoparticles with silica, *Ultrason. Sonochem.*, 17(1), 193–99.
2. DeNardo G. L., DeNardo S. J. (2008), Turning the heat on cancer, *Cancer Biother Radiopharm*, 23(6), 671–80.
3. Dunlop D. J., Özdemir Ö. (1997), *Rock Magnetism: Fundamentals and Frontiers*, Cambridge: Cambridge University Press. 131 p. 1st ed.
4. Fajaroh F., Setyawan H., Widiyastuti W., Winardi S. (2012), Synthesis of magnetite nanoparticles by surfactant-free electrochemical method in an aqueous system, *Adv. Powder Technol.*, 23(3), 328–33.
5. Giustini A. J., Petryk A. A., Cassim S. M., Tate J. A., Baker I,. Hoopes P. J. (2013), Magnetic nanoparticle hyperthermia in cancer treatment, *Nano Life*, 1, 1–23.

6. Harrison R. J., Dunin-Borkowski R. E., Putnis A. (2002), Direct imaging of nanoscale magnetic interactions in minerals, *Proc. Natl. Acad. Sci. U. S. A.*, 99(26), 16556–61.
7. Huang H. S., Hainfeld J. F. (2013), Intravenous magnetic nanoparticle cancer hyperthermia, *Int. J. Nanomedicine*, 8, 2521–32.
8. Jiang W., Lai K. L., Hu H., Zeng X. B., Lan F., Liu K. X., Wu Y., Gu Z. W. (2011), The effect of $[Fe^{3+}]/[Fe^{2+}]$ molar ratio and iron salts concentration on the properties of superparamagnetic iron oxide nanoparticles in the water/ethanol/toluene system, *J. Nanoparticle Res.*, 13(10), 5135–45.
9. Mascolo M. C., Pei Y., Ring T. A. (2013), Room Temperature Co-Precipitation Synthesis of Magnetite Nanoparticles in a Large ph Window with Different Bases, *Materials (Basel).*, 6(12), 5549–67.
10. McCabe W., Smith J., Harriott P. (1993), *Unit Operations of Chemical Engineering*, New York: McGraw-Hill. 884-899 p. 5th ed.
11. Nyborg W. L. (1965), Acoustic streaming, *Phys. Acoust.*, 2(Pt B), 265.
12. Patterson A. L. (1939), The Scherrer formula for X-ray particle size determination, *Phys. Rev.*, 56(10), 978–81.
13. Revia R. A., Zhang M. (2016), Magnetite nanoparticles for cancer diagnosis, treatment, and treatment monitoring: Recent advances, *Mater. Today*, 19(3), 157–68.
14. Scherrer P. (1918), Nachrichten von der Gesellschaft der Wissenschaften zu Göttingen, *Math. Klasse*, 2, 98–100.
15. Shirinova H., Di Palma L., Sarasini F., Tirill J., Ramazanov M. A., Hajiyeva F., Sannino D., Polichetti M., Galluzzi A. (2016), Synthesis and characterization of magnetic nanocomposites for environmental remediation, *Chem. Eng. Trans.*, 47, 103–8.
16. Singh A. K. (2005), *Advanced x-ray techniques in research and industry*, IOS Press
17. Vikesland P., Rebodos R., Bottero J-Y., Rose J., Masion A. (2016), Aggregation and Sedimentation of Magnetite Nanoparticle Clusters, *Environ. Sci. Nano*, 3, 567–77.
18. Wasilewski P., Kletetschka G. (1999), Lodestone: Natures only permanent magnet-What it is and how it gets charged, *Geophys. Res. Lett.*, 26(15), 2275–78.
19. Wen B., Lampe J. N., Roberts A. G., Atkins W. M., Rodrigues A. D., Nelson S. D. (2007), Definitions and Description of Nonthermal Mechanisms, *J Ultrasound Med.*, 454(1), 42–54.
20. Woo K., Hong J., Choi S., Lee H., Ahn J., Kim C.S., Lee S. W. (2004), Easy Synthesis and Magnetic Properties of Iron Oxide Nanoparticles, *Chem. Mater.*, 16(14), 2814–18.
21. Zhang Z., Zhou F., Lavernia E. J. (2003), On the analysis of grain size in bulk nanocrystalline materials via X-ray diffraction, *Metall. Mater. Trans. a-Physical Metall. Mater. Sci.*, 34A(6), 1349–55.